The Astrophysical Journal, 706:844–850, 2009 November 20 doi:10.1088/0004-637X/706/1/844

SOLAR ENERGETIC-PARTICLE RELEASE TIMES IN HISTORIC GROUND-LEVEL EVENTS

Donald V. Reames
Institute for Physical Science and Technology, University of Maryland, College Park, MD 20742, USA; dvreames@umd.edu
Received 2009 July 28; accepted 2009 October 14; published 2009 November 5

ABSTRACT

Ground-level events (GLEs) are large solar energetic-particle events with sufficiently hard spectra for GeV protons to be detected by neutron monitors at ground level. For each of 30 well-observed historic GLEs from four solar cycles, extending back to 1973, I have plotted onset times versus velocity^{-1} for particles observed on the *IMP-7* and *8*, *ISEE-3*, *Wind*, and *GOES* spacecraft and by neutron monitors. A linear fit on such a plot for each GLE determines the initial solar particle release (SPR) time, as the intercept, and the magnetic path length traversed, as the slope, of the fitted line. Magnetic path lengths and SPR times are well determined by the fits and cannot be used as adjustable parameters to make particle and photon emission times coincide. SPR times follow the onsets of shock-induced type II radio bursts and the coronal height of the coronal mass ejection (CME)-driven shock at SPR time can be determined for GLEs spanning an interval of solar longitude of ∼140 deg. For a given GLE, all particle species and energies diverge from a single SPR point at a given coronal height and footpoint longitude of the field line to the Earth. These heights tend to increase with longitudinal distance away from the source, a pattern expected for shock acceleration. Acceleration for magnetically well-connected large GLEs begins at ∼2 solar radii, in contrast to non-GLEs that have been found to be strongly associated with shocks above ∼3 solar radii. The higher densities and magnetic field strengths at lower altitudes may be responsible for the acceleration of higher-energy particles in GLEs, while those GLEs that begin above $3R_S$ may compensate by having higher shock speeds. These results support the joint dependence of maximum particle energy on magnetic field strength, injected particle density, and shock speed, all predicted theoretically.

Key words: acceleration of particles – shock waves – Sun: coronal mass ejections (CMEs) – Sun: particle emission – Sun: radio radiation

Online-only material: color figures

1. INTRODUCTION

Some of the largest solar energetic particle (SEP) events accelerate GeV ions that produce sufficient intensities of secondary particles at ground-level neutron monitors to be detectible above the background produced by galactic cosmic rays (GCRs). Seventy ground-level events (GLEs), occurring between 1942 and 2006, have been identified and numbered and their properties have been reported (Cliver et al. 1982; Cliver 2006). The hard proton spectrum in GLEs makes them especially hazardous to astronauts and equipment in space. Protons of ∼150 MeV, which are orders of magnitude more intense than those at 1 GeV, can penetrate 20 g cm^{-2} of Al or 15.5 cm of water and are extremely difficult to shield. GeV protons produce enough secondaries in nuclear interactions to make shielding counterproductive. Thus, understanding where, when, and how particle acceleration takes place is of practical as well as astrophysical interest.

In their classic review of GLEs, Cliver et al. (1982) compared particle onset times with Hα, radio, and X-ray observations in the solar source events. They found that the first relativistic protons were released as much as ∼30 minutes after the earliest photons from the flash phase of the associated flare. They concluded: "To account for these observations, we suggest a picture in which the earliest observed particles are injected when an outward moving acceleration region at a shock front intersects the open field lines connecting to Earth." The idea of particle acceleration at a shock wave driven outward by a coronal mass ejection (CME) in large SEP events is now widely accepted (see reviews Reames 1990, 1995, 1999, 2002; Kahler 1992, 1994, 2001; Gosling 1993; Lee 1997, 2005; Tylka 2001; Tylka et al. 2005). In these papers, the large, CME-associated "gradual" SEP events are distinguished from the smaller "impulsive" events associated with flares by the physical mechanism of acceleration.

Alternatively, however, one could imagine that the late onset times of the GeV protons in GLEs occur because the particles traverse a long path length following the magnetic field line from the source to the Earth. There is clear evidence of path lengths greater than the nominal 1.2 AU along the Parker spiral. Magnetic flux tubes may be mapped by tracking the frequency and direction of kilometric type III emission by electrons streaming outward from the Sun (e.g., Reames & Stone 1986). These maps show large departures from the Parker spiral. Also, studies of onset timing of impulsive electron events inside magnetic clouds show path lengths varying from ∼1.2 AU near the center of the cloud to ∼3 AU at its periphery (Larson et al. 1997) as expected for the twisted flux-rope topology of magnetic clouds. There can be little doubt that CMEs distort the interplanetary field enough to force newly accelerated particles to follow paths considerably greater than 1.2 AU.

Relativistic particles, that take ∼8 minutes to travel 1 AU, would take ∼16 minutes to travel a distorted path length of 2 AU, hence they might be accelerated 8 minutes earlier than otherwise expected. However, this long path length has consequences for slower particles which must be accelerated before those at 1 GeV. Thus, for example, 10 MeV protons that travel about 1 AU hr^{-1} would take 2 hr to travel a path length of 2 AU, a difference in the onset time of 1 hr that would be extremely obvious. In fact, observations of the onset times of particles of different velocities may be used to directly determine both the path length to the source and the solar particle release (SPR)

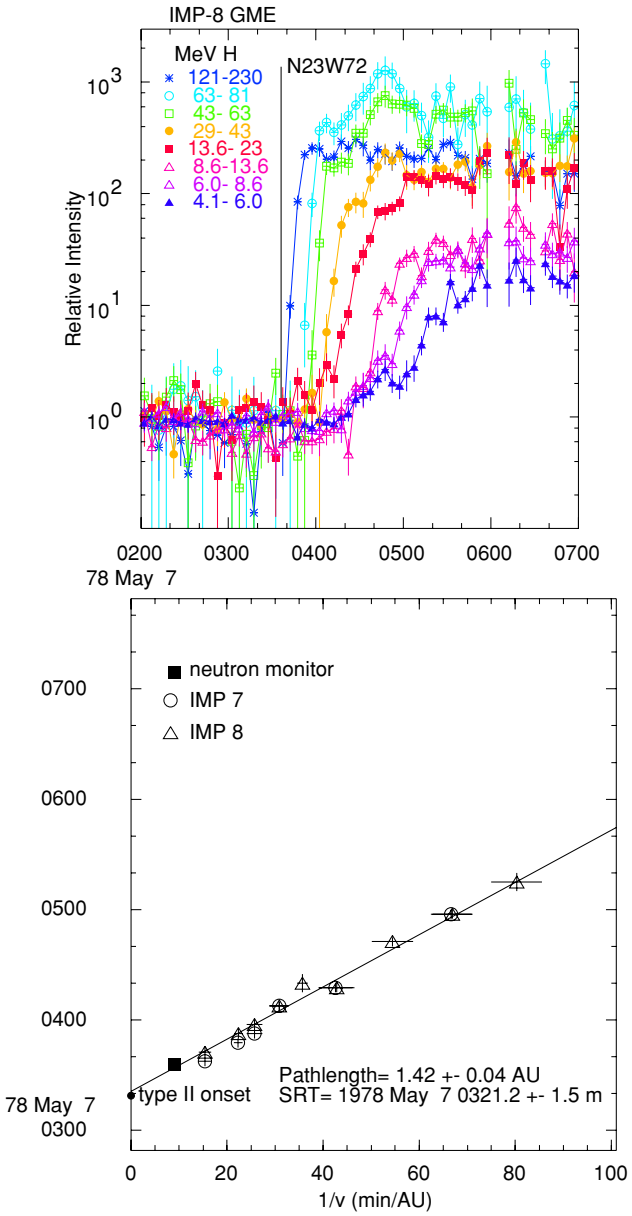

Figure 1. Upper panel shows intensities of protons vs. time at *IMP-8* for the indicated energy intervals during the GLE of 1978 May 7. The lower panel shows a velocity dispersion plot, onset times vs. v^{-1}, for protons intervals on *IMP-7* and *IMP-8* and for the neutron monitors. The least-squares fit line determines the magnetic path length as the slope and the SPR time as the intercept, both listed in the figure.

(A color version of this figure is available in the online journal.)

time. Linear fits on plots of the onset time versus the inverse of the particle velocity, v^{-1}, have the path length as the slope and the SPR time as the intercept. These plots of the velocity dispersion have been used for many years to study impulsive SEP events (Lin et al. 1981; Reames et al. 1985). More recently, Tylka et al. (2003) compared the velocity dispersion of impulsive events with that of GLEs. For the impulsive events, the SPR times coincided with hard X-ray peak times, but for GLEs the SPR times occurred as much as 25 minutes after the 4–7 MeV gamma-ray peaks. The results for the impulsive events prove the technique while those for GLEs confirm the conclusions of Cliver et al. (1982).

In a recent paper, Reames (2009, hereinafter paper I), extended the work of Tylka et al. (2003) and determined the SPR times of 13 of the 16 GLEs during solar cycle 23. Plotting the height of the CMEs at the SPR times as a function of solar longitude, Paper I showed a pattern of height that was low for events at magnetically well-connected solar longitudes but increased for events observed on the flanks of the CMEs. Generally, the height at SPR time for the 13 events was between 2 and 6 solar radii (R_S).

In this paper, the work of Paper I is extended back in time by measuring, where possible, onset times of particles for historic GLE events in solar cycles 20, 21, and 22, from 1973 to 1994. Data for determination of the proton velocity dispersion come primarily from the similar instruments of the Goddard Space Flight Center on the *IMP-7* and *IMP-8* spacecraft as well as neutron monitor data. However, data from *ISEE-3* and high-energy data from the NOAA *GOES* spacecraft were also used. Data from most of these sources were described in detail in Paper I. Neutron monitor onset times from the earlier events are listed in Cliver et al. (1982). It has not been possible to measure all events during the study period because of data gaps during many events and instrument saturation during a few. Also, since many of the events did not have CME observations I was forced to fall back on shock transit speeds to determine the shock height at SPR time as described in Paper I. Shock transit speeds are determined from type II onset time to the time of sudden commencement at the Earth. For GLEs with CME measurements, the speeds tabulated by Cliver (2006) were used.

2. ANALYSIS OF SEP ONSET TIMES

The first particles of a given velocity to arrive at the Earth from a source near the Sun are minimally scattered particles that have been focused into a narrow cone of pitch angle by the diverging magnetic field. As time increases, greater numbers of particles arrive in a wider cone of pitch angles and the intensity rises and eventually flattens toward a maximum. The measured onset time depends upon the sensitivity of an instrument to particles of given velocity and upon the level of background. Pitch-angle scattering slows the rise in intensity and delays the apparent onset, a process that has been modeled for large SEP events (Sáiz et al. 2005, see also Ng et al. 2003). The possible effects of pitch-angle scattering have been discussed at length in Paper I. The analysis technique and onset data for many events have also been shown and discussed in Paper I.

The upper panel of Figure 1 shows the intensities of protons of various energies measured by the Goddard Medium Energy (GME) instrument on the *IMP-8* spacecraft for GLE 31 on 1978 May 7. The lower panel of the figure shows the onset times versus inverse velocity for protons from several energy intervals at *IMP-7* and *IMP-8* and for neutron monitors. The least-squares fit line determines the magnetic path length as the slope and the SPR time as the intercept, both of which are listed in the figure. Measurements on the two spacecraft are in good agreement here as in all events.

Figure 2 shows data for GLE 34 on 1981 April 10, for which only data from *IMP-8* are available. Nevertheless, the path length and SPR time are reasonably well determined for this event. In this event, the neutron monitor increase is only 2% above the GCR background so the onset time is poorly determined. Actually, over half of the GLEs have neutron monitor increase of <10% of GCRs, so they provide poor timing information.

Figure 3 shows velocity dispersion fits for three more GLEs spanning a significant time interval and showing different combinations of spacecraft data. GLE 26 on 1973 April 29

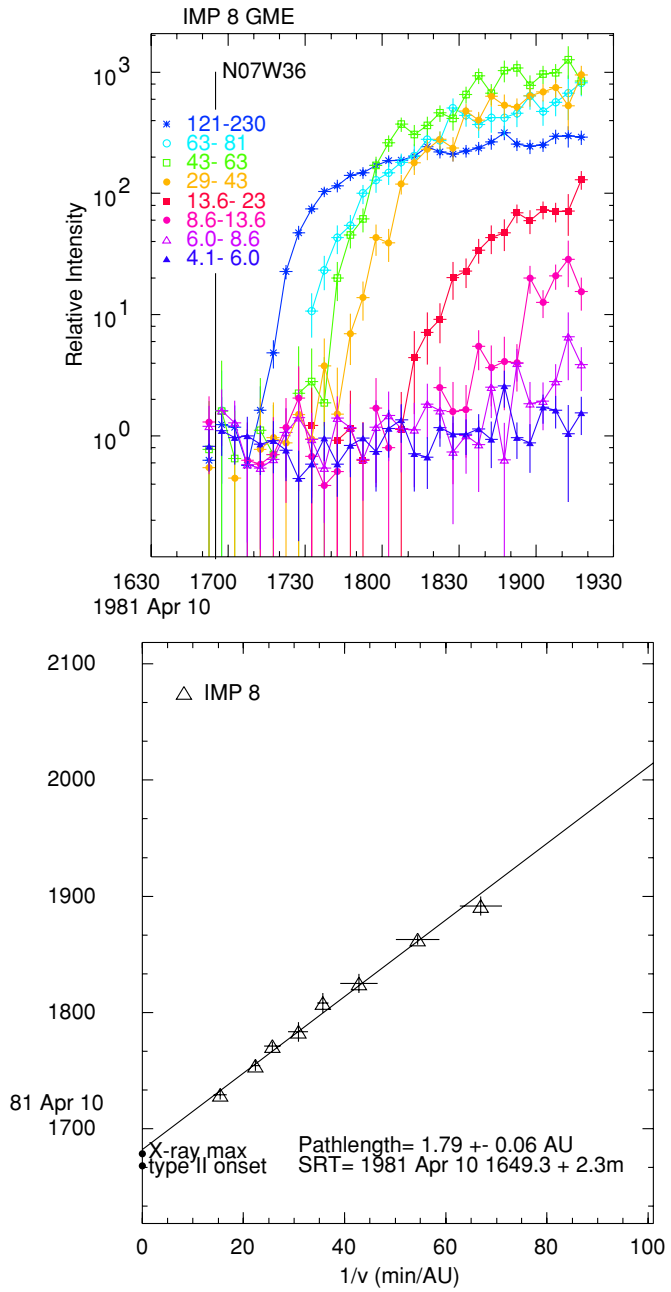

Figure 2. Upper panel shows intensities of protons vs. time at *IMP-8* for the indicated energy intervals during the GLE of 1981 April 10. The lower panel shows a velocity dispersion plot, onset times vs. v^{-1}, for the protons intervals on *IMP-8*. The least-squares fit line determines the magnetic path length as the slope and the SPR time as the intercept, both listed in the figure.

(A color version of this figure is available in the online journal.)

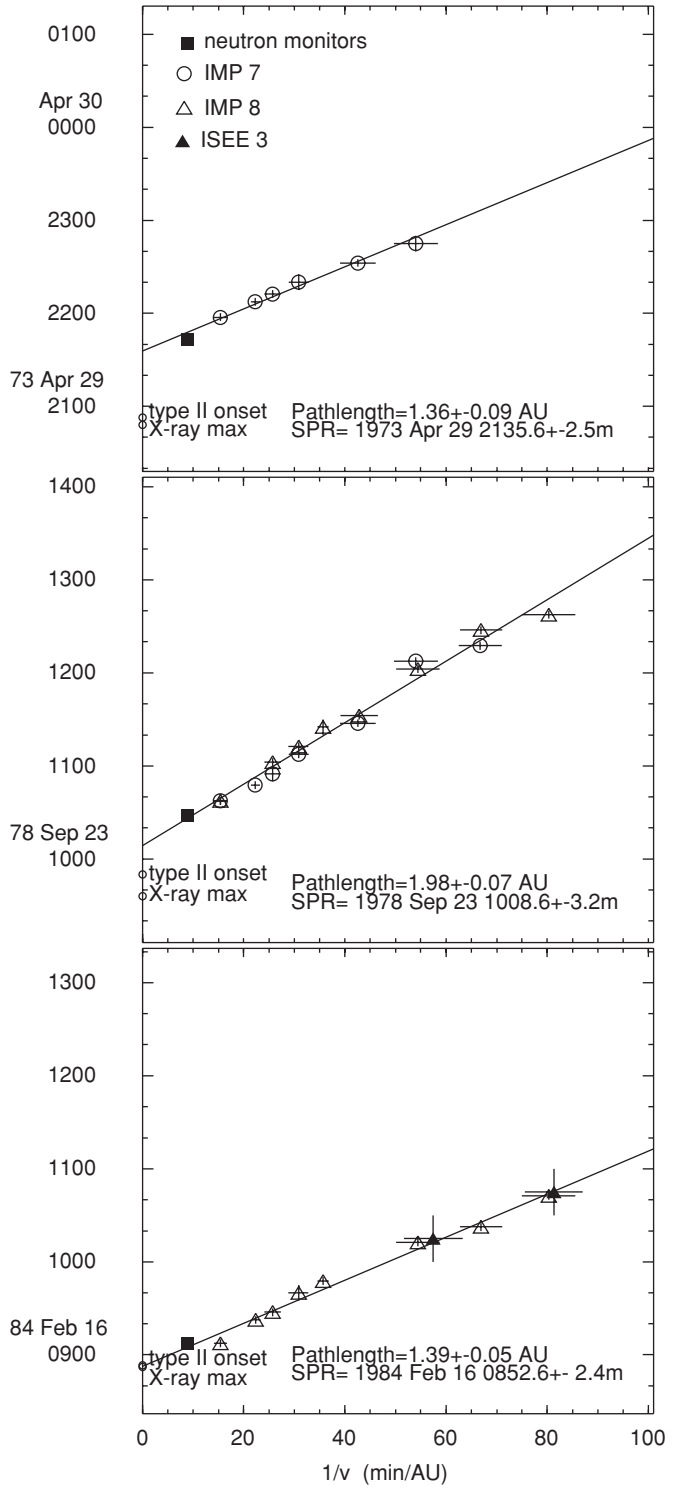

Figure 3. Velocity dispersion plots are shown for the GLEs of 1973 April 29, 1978 September 23, and 1984 February 16, involving data from the sources listed. Fitted path lengths and SPR times are listed.

is the earliest event we can study and is covered only by *IMP-7*, GLE 32 on 1978 September 23 is covered by both *IMP-7* and *IMP-8*, and GLE 39 on 1984 February 16 is covered by *IMP-8* and *ISEE-3*.

The properties of all the GLEs in this study, including those from Paper I, are shown in Table 1. Of the total of 45 GLEs since 1973, SPR times and path lengths have been determined for 30 GLEs. Of these, 26 have either CME speeds or shock transit speeds, so the shock height at SPR time can be determined. Individual columns in the table are (1) the GLE number, (2) the initial SPR time at the Sun, (3) the magnetic path length, (4) the source latitude and longitude, (5) the shock speed (or CME speed when available), (6) Dt, the SPR time minus the type II onset time at the Sun, (7) R(SPR), the radial height of the CME-driven shock at the initial SPR time, (8) $\boldsymbol{\phi}$, the source longitude relative to the footpoint of the field line to the Earth, and (9) the peak neutron monitor intensity as a percentage of the GCR intensity.

Note that the magnetic path length of the particles is well determined by the velocity–dispersion plots shown here and in

Table 1
Solar Release Properties of GLEs

GLE	Initial SPR Time (UT at Sun)	Path Length (AU)	Source Location	V_{shock} (km s^{-1})	Dt (minutes)	R(SPR) (R_S)	Φ (deg)	GCR (%)
26	1973 Apr 29 2135.6 ± 2.4	1.36 ± 0.09	N13W73	920	42.9 ± 2.4	4.9 ± 0.2	36.7 ± 0.6	3
27	1976 Apr 30 2107.6 ± 2.6	1.37 ± 0.06	S08W46	910	9.9 ± 2.6	2.3 ± 0.2	−6.9 ± 1.2	4
28	1977 Sep 19 1034.7 ± 2.1	2.45 ± 0.07	N08W57	720	8.0 ± 2.1	2.0 ± 0.1	−1.1 ± 1.5	2
29	1977 Sep 24 0548.6 ± 2.6	2.16 ± 0.07	N10W120	...	1.9 ± 2.6	...	73.5 ± 0.9	6
30	1977 Nov 22 1014.5 ± 3.5	1.31 ± 0.09	N24W40	560	23.8 ± 3.5	2.6 ± 0.2	−32.6 ± 2.3	25
31	1978 May 7 0321.2 ± 1.5	1.42 ± 0.04	N23W72	...	2.5 ± 1.5	...	19.2 ± 1.2	80
32	1978 Sep 23 1008.6 ± 3.2	1.98 ± 0.07	N35W50	910	18.9 ± 3.2	3.0 ± 0.3	−14.6 ± 1.8	8
33	1979 Aug 21 0616.0 ± 3.5	1.66 ± 0.12	N17W40	690[a]	9.3 ± 3.5	2.0 ± 0.2	1.3 ± 0.7	6
34	1981 Apr 10 1649.3 ± 2.3	1.97 ± 0.06	N07W36	918	8.5 ± 2.3	2.2 ± 0.2	−23.6 ± 1.5	2
37	1982 Nov 26 0302.1 ± 5.8	1.96 ± 0.15	S12W87	890	36.4 ± 5.8	4.3 ± 0.4	51.2 ± 2.8	6
38	1982 Dec 7 2343.4 ± 3.8	1.78 ± 0.10	S19W86	1250[a]	8.2 ± 3.8	2.4 ± 0.4	24.8 ± 1.6	56
39	1984 Feb 16 0852.6 ± 2.4	1.39 ± 0.05	∼W130	1200[a]	0.2 ± 2.4	1.5 ± 0.2	72.5 ± 5.8[b]	72
42	1989 Sep 29 1126.9 ± 3.1	2.49 ± 0.13	∼W100	1828[a]	9.5 ± 3.1	3.0 ± 0.5	42.5 ± 5.8[b]	270
43	1989 Oct 19 1245.7 ± 3.1	1.43 ± 0.11	S25E09	...	5.0 ± 3.1	...	−52.8 ± 0.8	53
46	1989 Nov 15 0654.4 ± 3.5	1.31 ± 0.15	N11W28	827	5.7 ± 3.5	1.9 ± 0.2	−38.5 ± 1.9	5
47	1990 May 21 2214.1 ± 2.2	2.19 ± 0.08	N34W37	539	10.4 ± 2.2	2.0 ± 0.1	−6.8 ± 1.7	14
49	1990 May 26 2057.0 ± 8.2	1.50 ± 0.27	∼W100	...	17.3 ± 8.2	...	42.5 ± 5.8[b]	8
56	1998 May 2 1346.7 ± 2.7	1.24 ± 0.04	S15W15	938[a]	17.0 ± 2.7	2.9 ± 0.2	−23.9 ± 0.1	7
57	1998 May 6 0803.5 ± 1.6	1.11 ± 0.02	S15W64	1099[a]	5.8 ± 1.6	2.0 ± 0.2	14.1 ± 0.6	5
58	1998 Aug 24 2232.1 ± 4.6	1.55 ± 0.04	N35E09	1275	38.4 ± 4.6	5.7 ± 0.5	−62.1 ± 0.2	5
59	2000 Jul 14 1016.5 ± 1.8	1.71 ± 0.03	N22W07	1674[a]	7.6 ± 1.8	2.6 ± 0.3	−30.8 ± 0.1	29
60	2001 Apr 15 1347.7 ± 1.7	1.59 ± 0.01	S20W84	1199[a]	9.0 ± 1.7	2.4 ± 0.2	38.2 ± 0.5	57
61	2001 Apr 18 0224.3 ± 3.2	1.80 ± 0.10	∼W115	2465[a]	15.6 ± 3.2	4.8 ± 0.7	67.1 ± 1.5	14
63	2001 Dec 26 0520.6 ± 3.7	1.64 ± 0.06	N08W54	1446[a]	16.9 ± 3.7	3.6 ± 0.5	−7.2 ± 0.7	7
64	2002 Aug 24 0100.1 ± 2.8	2.16 ± 0.05	S02W81	1913[a]	5.4 ± 2.8	2.4 ± 0.5	20.9 ± 0.8	5
65	2003 Oct 28 1105.1 ± 1.8	1.38 ± 0.03	S16E08	2459[a]	13.1 ± 1.8	4.3 ± 0.4	−36.9 ± 0.2	8
66	2003 Oct 29 2055.6 ± 5.8	1.75 ± 0.09	S15W02	2029[a]	23.9 ± 5.8	5.7 ± 1.0	−35.6 ± 3.1	5
67	2003 Nov 2 1713.8 ± 2.1	2.01 ± 0.04	S14W56	2598[a]	8.1 ± 2.1	3.3 ± 0.5	12.4 ± 1.2	7
69	2005 Jan 20 0639.5 ± 1.2	1.19 ± 0.02	N12W58	3242[a]	3.8 ± 1.2	2.6 ± 0.3	31.4 ± 0.3	270
70	2006 Dec 13 0234.0 ± 3.7	1.72 ± 0.05	S06W26	1774[a]	15.3 ± 3.7	3.8 ± 0.6	−9.9 ± 0.1	92

Notes.
[a] CME speeds.
[b] solar wind speed of 400 km s^{-1} assumed.

Paper I. The path length is not an adjustable parameter that can be increased arbitrarily to make the SPR time coincide with some earlier peak in photon emission at the Sun.

3. SPATIAL DISTRIBUTION OF THE EVENT SOURCES

To estimate the location of each CME-driven shock at initial SPR time, I follow the procedure that was used and verified in Paper I. This assumes that a typical metric type II onset frequency of ∼100 MHz corresponds to a radius of ∼1.5R_S (e.g., Kundu 1965) where shock formation begins. Subsequently, the CME or shock speed multiplied by the delay of the SPR time after type II onset then gives the height of the shock corresponding to the initial SPR time. This procedure allows determination of the SPR height when CME observations are not available. The result compared favorably with heights determined from CME height–time plots in Paper I.

Figure 4 shows the radial height of the shock at SPR time, R(SPR), versus ϕ, the solar source longitude relative to the footpoint of the field line to the Earth. The GLE number is shown beside each point. In an attempt to characterize the first-order behavior of the data in this figure, I have performed a linear least-squares fit of R(SPR) versus ϕ^2, which appears as a parabola in Figure 4. The fit gives $R(\mathrm{SPR}) = 2.08 + (\phi/36.^{\circ}4)^2$. Event 39 (1984 February 16) was omitted from this fit; this event is alleged to originate far (40°) behind the west limb, the solar wind speed is not available to determine the footpoint longitude, and even the type II emission might be generated late, near the limb, rather than earlier at the backside source.

The fit in Figure 4 emphasizes the fact that the events with the smallest errors tend to cluster along the lower boundary of the distribution. Unfortunately, when one looks at a distribution of plotted points, it is the points with the largest errors that stand out, while the most accurate points are smaller and more difficult to see. The weighted least-squares fit tends to compensate for this optical illusion, since the points with the smallest errors are favored. The fitted curve is most useful because it tends to draw ones attention to the distribution of the most precise points in the plot. However, we shall see that all SEP events do not lie on a single curve.

While the fitted curve in Figure 4 has no direct physical basis, and is only a first approximation to CME shapes and shock conditions that vary widely, there does seem to be a tendency for many of the events to cluster along it. This is even more evident when we replace the GLE number with the GLE intensity as a percentage of GCR intensity, as shown in Figure 5. Of the 10 GLEs with intensities >10% of GCRs, 8 of them cluster along just beneath the fitted curve.

4. ACCELERATION TIME

Low-energy particles must be accelerated before those at high energy. Therefore, a fit to a velocity dispersion plot containing only lower-energy data might determine an SPR time that is earlier than the one containing high-energy data. As an

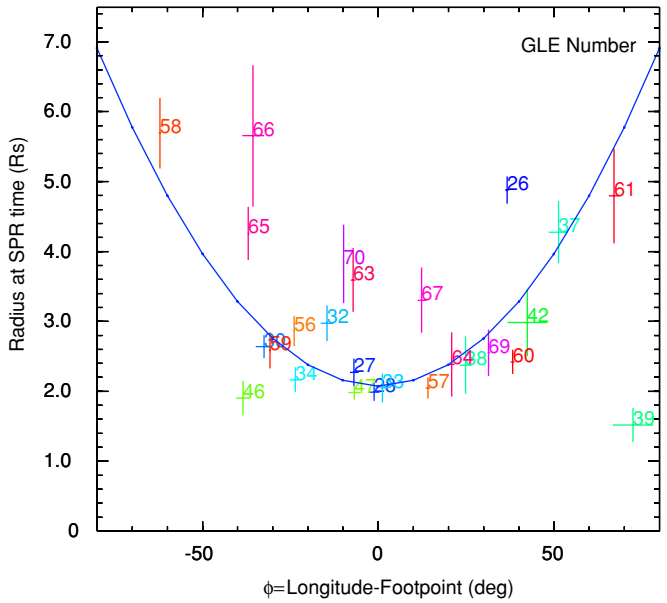

Figure 4. Radial height of the shock at SPR time, R(SPR), is shown vs. $\boldsymbol{\phi}$, the solar source longitude relative to the footpoint of the field line from the Earth for 26 GLEs. The parabola is a first-order fit of R(SPR) vs. $\boldsymbol{\phi}^2$, namely $R = 2.08 + (\boldsymbol{\phi}/36.^{\circ}4)^2$, excluding GLE 39 (see the text).

(A color version of this figure is available in the online journal.)

attempt to make a crude estimate of the acceleration time, I have generated an SPR time on a plot containing data of <100 MeV and subtracted it from the SPR time for the full data set containing ~1 GeV data. Only 16 events with complete energy coverage were used. The mean acceleration time from <100 MeV to ~1 GeV by this measure is -2.7 ± 3.7 minutes, indicating that it is not possible to measure a realistic time, but a limit can be set to less than ~4 minutes.

It is unclear what role wave trapping plays here (e.g., Ng & Reames 2008; Ng et al. 2003). Accelerated particles take time to fight their way out of the enhanced upstream wave field. Could 10–100 MeV protons, though accelerated earlier, take more time to escape the source relative to GeV protons, which are accelerated later?

5. DISCUSSION

One of the more striking results of this study is the low SPR altitude of $2.1R_S$ or less, appropriate for large GLEs that are magnetically well connected. This contrasts with the conclusions of Cliver et al. (2004) that most SEP events (i.e., non-GLEs) are strongly associated with shocks above $\sim 3R_S$. In fact, most SEP events are associated with type II emission that occurs in the decametric–hectometric range (1–14 MHz). This lower frequency range corresponds to higher altitudes of $3–10R_S$ (e.g., Kundu 1965).

The association of high-energy particles with lower altitudes, and increased density and magnetic field strength, might have been anticipated from theoretical considerations. Zank et al. (2000) found that the maximum particle energy at a shock increased with the magnetic field strength, B, and the upstream plasma speed in the rest frame of the shock. Separately, Ng & Reames (2008) studied the time dependence of the shock acceleration in the corona. For a quasi-parallel shock beginning at $3.5R_S$, they found an acceleration time of ~10 minutes. They also found that the time required for particles to reach high energy at a shock decreases nonlinearly with the number of particles being accelerated since more particles generate more waves and, hence, more scattering back and forth across the shock up to the Bohm limit where the scattering mean free path equals the gyro radius. This suggests much more rapid acceleration at lower altitudes.

The dependence of the maximum particle energy on both B and shock speed, $V_{\rm shock}$, described by Zank et al. (2000), suggests a possible tradeoff between the two variables to produce a GLE. In Figure 6, we investigate this possibility on the plot of R(SPR) versus $\boldsymbol{\phi}$ by allowing the point size and color to vary with $V_{\rm shock}$. It can be seen that many of the GLEs with values of R(SPR) that lie above the fitted parabola have high

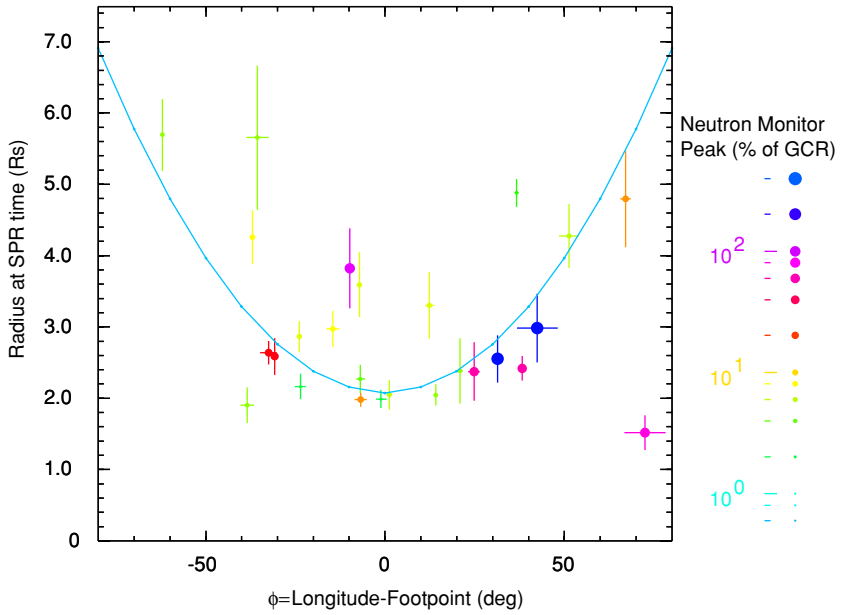

Figure 5. R(SPR) vs. $\boldsymbol{\phi}$ is shown for GLEs, as in Figure 4, with the point size and color indicating the GLE intensity as a percentage of GCR intensity. Most (8 out of 10) of the largest GLEs cluster along below the fitted parabola.

(A color version of this figure is available in the online journal.)

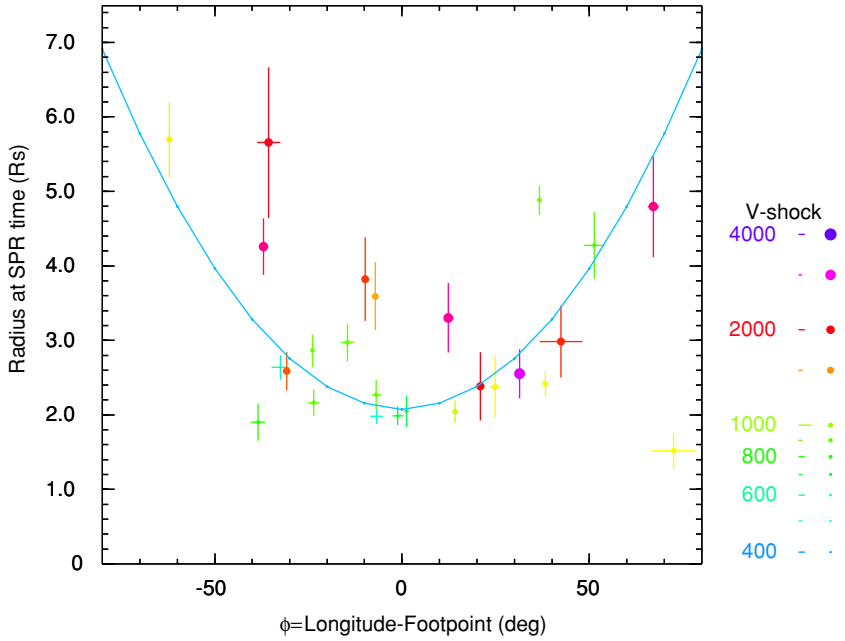

Figure 6. R(SPR) vs. ϕ is shown for GLEs, as in Figure 4, with the point size and color indicating the shock speed. Seven of the nine GLEs with R(SPR) $>3R_S$ have shock speeds above 1200 km s^{-1}.

(A color version of this figure is available in the online journal.)

shock speeds. In fact, of the total of nine GLEs that lie above $3R_S$ in the figure, seven have shock speeds >1200 km s^{-1}.

Note, therefore, that all events should not lie along the single fitted curve in Figures 4–6. The curve appears to define the locus of the strongest GLEs deep in the corona where the magnetic fields and densities are high while weaker SEP events begin at greater altitude, becoming GLEs only when the shock speed is very high.

As a fast CME drives radially outward from a region above the solar surface, a strong shock wave forms when the Alfvén speed ahead of the CME falls below the CME speed. The Alfvén speed (and fast-mode speed) decreases rapidly with radial distance to a minimum of ~200 km s^{-1} at ~$1.5R_S$ (~100 MHz) then rises to a maximum of ~500–700 km s^{-1} at ~$3R_S$ (~14 MHz) and decreases thereafter (Mann et al. 1999, 2003; Gopalswamy et al. 2001; Vršnak et al. 2002). It would not be surprising for the fast shocks associated with these GLEs to form near $1.5R_S$ and begin to accelerate particles somewhere above $2R_S$. CMEs encounter this radius and the shocks form over a broad front, depending upon the width of the CME. However, at the flanks of the CME, the shock does not form at more distant longitudes until the CME expands to higher altitudes.

6. CONCLUSIONS

Using onset times for various ions of various velocities, it has been possible to determine the initial SPR times and magnetic path lengths for 30 of the 45 GLE events in solar cycles 20, 21, 22, and 23, including the events from Paper I. From this work, I draw the following conclusions:

1. SPR times and magnetic path lengths from the Sun to the Earth are well determined in each GLE event, independently of connection longitude, for all particle species and energies. The path length is not an adjustable parameter that may be increased arbitrarily to make particle and photon emission times coincide.
2. The initial SPR times occur after the onset times of type II emission in all events.
3. When the SPR times are interpreted in terms of height of initial acceleration in the corona, the pattern of height versus longitude is generally consistent with shock acceleration over a broad spatial region with heights, rising on the flanks of the shock.
4. Particles from magnetically well-connected GLEs are typically accelerated at a radius of ~$2R_S$ while non-GLEs are associated with shocks above $3R_S$. The higher densities and magnetic field strengths at lower altitudes may be required to produce the higher-energy particles that characterize GLEs.
5. GLEs where acceleration begins above $3R_S$ are likely to have higher shock speeds (>1200 km s^{-1}), corroborating the joint dependence of maximum particle energy on both field strength and shock speed (Zank et al. 2000).
6. The acceleration time from <100 MeV to ~1 GeV is probably less than ~4 minutes.

I thank Nand Lal and Bryant Heikkila for their assistance in obtaining 5-minute averaged data from *IMP-7* and *IMP-8*. I also thank Ed Cliver, Frank McDonald, Chee Ng, Allan Tylka, and Gary Zank for helpful discussions and for their comments on this work.

This work was funded by the NASA grant NNX08AQ02G.

REFERENCES

Cliver, E. W. 2006, ApJ, 639, 1206
Cliver, E. W., Kahler, S. W., & Reames, D. V. 2004, ApJ, 605, 902
Cliver, E. W., Kahler, S. W., Shea, M. A., & Smart, D. F. 1982, ApJ, 260, 362
Gopalswamy, N., Lara, A., Kaiser, M. L., & Bougeret, M. L. 2001, J. Geophys. Res., 106, 25261
Gosling, J. T. 1993, J. Geophys. Res., 98, 18937
Kahler, S. W. 1992, ARA&A, 30, 113
Kahler, S. W. 1994, ApJ, 428, 837
Kahler, S. W. 2001, J. Geophys. Res., 106, 20947

Kundu, M. R. 1965, Solar Radio Astronomy (New York: Wiley)
Larson, D. E., et al. 1997, Geophys. Res. Lett., 24, 1911
Lee, M. A. 1997, in Geophys. Monograph 99, Coronal Mass Ejections, ed. N. Crooker, J. A. Jocelyn, & J. Feynman (Washington, DC: AGU Press), 227
Lee, M. A. 2005, ApJS, 158, 38
Lin, R. P., Potter, D. W., Gurnett, D. A., & Scarf, F. L. 1981, ApJ, 251, 363
Mann, G., Aurass, H., Klassen, A., Estel, C., & Thompson, B. J. 1999, in Plasma Dynamics and Diagnostics in the Solar Transition Region and Corona, ed. J.-C. Vial & B. Kaldeich-Schurmann (ESA SP-446; Noordwijk: ESA), 477
Mann, G., Klassen, A., Aurass, H., & Classen, H. T. 2003, A&A, 400, 329
Ng, C. K., & Reames, D. V. 2008, ApJ, 686, L123
Ng, C. K., Reames, D. V., & Tylka, A. J. 2003, ApJ, 591, 461
Reames, D. V. 1990, ApJS, 73, 235
Reames, D. V. 1995, Rev. Geophys. (Suppl.), 33, 585
Reames, D. V. 1999, Space Sci. Rev., 90, 413
Reames, D. V. 2002, ApJ, 571, L63
Reames, D. V. 2009, ApJ, 693, 812 (Paper I)
Reames, D. V., & Stone, R. G. 1986, ApJ, 308, 902
Reames, D. V., von Rosenvinge, T. T., & Lin, R. P. 1985, ApJ, 292, 216
Sáiz, A., Evenson, P., Ruffolo, D., & Bieber, J. W. 2005, ApJ, 626, 1131
Tylka, A. J. 2001, J. Geophys. Res., 106, 25333
Tylka, A. J., Cohen, C. M. S., Dietrich, W. F., Lee, M. A., Maclennan, C. G., Mewaldt, R. A., Ng, C. K., & Reames, D. V. 2005, ApJ, 625, 474
Tylka, A. J., et al. 2003, Proc. 28th Int. Cosmic Ray Conf., Vol. 6 (Tsukuba), 3305
Vršnak, B., Magdalenić, J., Aurass, H., & Mann, G. 2002, A&A, 396, 673
Zank, G. P., Rice, W. K. M., & Wu, C. C. 2000, J. Geophys. Res., 105, 25079